

Thermal wave imaging of electrically heated microstructures

P. Voigt, J. Hartmann, and M. Reichling^{a)}

Fachbereich Physik, Freie Universität Berlin, Arnimalle 14, 14195 Berlin, Germany

(Received 7 March 1996; accepted for publication 15 April 1996)

The thermoreflectance technique is applied for imaging electric current distributions and thermal transfer in a temperature reference resistor heated by an alternating current. High-frequency scans (30 kHz) allow imaging of the current density distribution in conducting strips of the resistor while scans of amplitude and phase of the surface temperature variation at lower frequencies reveal plane, cylindrical, and spherical thermal waves. We investigate wave dimensionality as a function of heating geometry and thermal length, and present a simple method allowing a quantitative thermal analysis by exploiting the phase profile of cylindrical thermal waves. © 1996 American Institute of Physics. [S0021-8979(96)11115-4]

I. INTRODUCTION

Due to their increasing compactness electronic micro-devices suffer from intensive heating limiting their lifetime. Therefore, thermal management, i.e., localizing and avoiding strong heat sources, plays an important role in the design of integrated circuits. A prerequisite for design optimization is analytical tools for the detection of hot spots. While the lateral resolution of steady-state infrared video techniques is insufficient to localize hot spots with micron resolution, photothermal and photoacoustic imaging techniques are well suited to monitor heat sources and diffusion.¹⁻³ In contrast to other photothermal techniques utilizing laser heating, the technique applied here is based on periodic Joule heating of an electrically conducting sample by an alternating current; the concept and data interpretation, however, are very similar to laser heating experiments.⁴⁻⁶ Photothermal methods are well established for the characterization of semiconducting materials and devices. Mandelis, Williams, and Siu⁷ monitored subsurface structures and electronic processes in an active transistor by thermal wave and plasma wave depth profiling using a deflection technique to measure the induced temperature change. Detailed studies on photothermal detection of doping features in silicon have been presented by Forget and Fournier.^{8,9} Of particular importance to quality testing is the imaging of temperature distributions in operating laser diodes^{10,11} and integrated circuits.¹²⁻¹⁵

The present work demonstrates the visualization of temperature oscillations due to modulated Joule heating in an arrangement of platinum conducting strips in a temperature reference resistor. By a variation of the ac frequency we aim to separate the contributions of local Joule heating and thermal waves and we study the role of thermal wave dimensionality. Cylindrical waves are utilized to measure heat transfer to the substrate by analyzing phase profiles.

II. EXPERIMENT

The experimental setup is outlined in Fig. 1. Its operation and performance is similar to other photothermal microscopes reported in the literature.¹⁶ Due to the thermoreflec-

tance effect the intensity of the reflected probe beam is modulated proportionally to the temperature oscillation on the irradiated spot induced by the electric current. Details of this technique are described elsewhere.¹⁷ The output signal of a function generator is amplified by a commercial audio amplifier to obtain an average heating power of about 2 W. In contrast to previously performed work³ we now use a commercial microscope to achieve a spot size of a few microns for the HeNe probe laser beam on the sample. After separation from the incident beam by a Faraday rotator the intensity of the reflected beam is measured by a photodiode. Phase-sensitive detection by a lock-in amplifier yields the amplitude of the temperature oscillation and its phase shift with respect to the heating power in arbitrary units. To obtain thermal images the sample is mounted on a motor driven translation stage allowing the test beam to scan the area of interest.

As a sample we chose a structure of platinum conduction strips on a Al₂O₃ substrate manufactured by Jumo (Fulda, Germany). The device is commercially used as a resistive thermometer (40 Ω at room temperature). The conducting strips with a thickness of 2 μm form a maze in which the electric current passes through loops, serpentines, and bottlenecks resulting in a very inhomogeneous current density distribution and a thermal pattern of hot spots and cold regions. Measurements were performed at frequencies ranging from 0.3 to 30 kHz.

III. BASIC PRINCIPLES OF CURRENT DENSITY IMAGING

Neglecting capacitance and induction effects in the circuit, we assume that the current density $j(\mathbf{r}, t)$ oscillates at any location \mathbf{r} with frequency ω and the same phase. The Joule heating power per unit volume resulting from the electric current density $j(\mathbf{r}, t) = j_0(\mathbf{r}, t) \sin(\omega t)$ can be split into a constant and an oscillating part,

$$\frac{dP(\mathbf{r}, t)_{\text{Joule}}}{dV} = \frac{J^2(\mathbf{r}, t)}{2\sigma} = \frac{j_0^2(\mathbf{r})}{2\sigma} + \frac{j_0^2(\mathbf{r})}{2\sigma} \exp(i2\omega t), \quad (1)$$

^{a)} Author to whom correspondence should be addressed; Electronic mail: reichling@math1.physik.fu-berlin.de

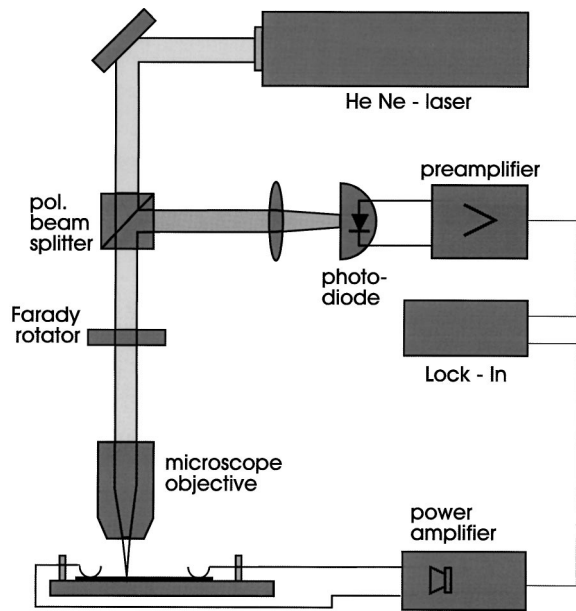


FIG. 1. Schematic view of the photothermal microscope.

where σ is the specific resistivity of the sample. To obtain the time-dependent temperature field in the sample each term in Eq. (1) can be used as a source term in the heat diffusion equation.¹⁸

The time-independent term $j_0^2(r)/2\sigma$ gives rise to a slowly varying temperature distribution in which spatial variations of the heating power are smeared out. In contrast, the oscillating term $[j_0^2(r)/2\sigma]\exp(i2\omega t)$ causes a pattern of thermal waves oscillating at twice the ac frequency carrying the information about local heating and heat diffusion from strongly heated regions. The decay of the heavily damped waves can roughly be described by the thermal diffusion length $L_{th} = \sqrt{2D/2\omega}$, where $D = \sqrt{\kappa/\rho c_p}$ is the thermal diffusivity combining the thermal conductivity κ with the specific heat c_p and the density ρ . L_{th} is the decay length of plane thermal waves, while attenuation is stronger for cylindrical and spherical wave geometries.

In general the temperature oscillation at a particular point is composed of a contribution due to local deposited heat and superimposed thermal waves from remote sources. The former contribution is proportional to $j_0^2(r)/\sigma$; while the latter reveals typical wavelike features such as decay in amplitude and an increasing phase lag as a function of distance from the source. Due to the frequency dependence of the thermal length, hot spots are best localized at high frequencies, while wave propagation can be monitored conveniently at low frequencies. Our test sample allows the study of thermal waves of different dimensionality that are depicted schematically in Fig. 2.

A conducting strip of length l , thickness h , and lateral size w larger than the thermal diffusion length causes a plane wave in the vertical direction [Fig. 2(a)]. To simplify the discussion we neglect the influence of the semicylindrical thermal waves at the edges. The wave originating from a conducting strip being narrower than the thermal length ($w < L_{th}$) can approximately be described by a cylindrical

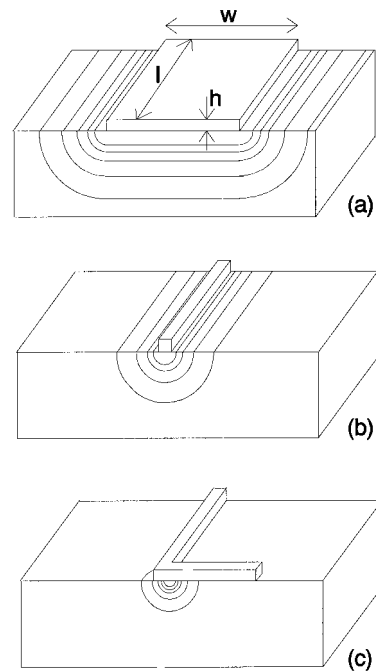


FIG. 2. Schematic representation of thermal waves originating from conducting strips of different geometry: (a) plane wave; (b) cylindrical wave; (c) spherical wave. In (c) only the dominant wave caused by the hot spot at the right angle is shown. Small letters denote strip dimensions.

wave [Fig. 2(b)]. Sharp bends in a conducting strip give rise to highly localized current densities and result in pointlike heat sources (hot spots) forming spherical waves [Fig. 2(c)].

We now present a theoretical basis for the correlation between photothermal amplitude and thermal wave dimensionality. For that purpose, consider a rectangular conducting strip carrying an ac electric current of amplitude I_0 , which gives rise to an ac current density $j_0 = I_0/wh$. The resulting modulated heating power deposited in the entire strip is

$$P = \frac{dP}{dV} w l h = \frac{I_0^2 l}{2\sigma w h}. \quad (2)$$

For one-dimensional heat flow the photothermal amplitude a is proportional to the heating power per unit area, i.e., $a \sim P/lw$. Using Eq. (2) we obtain

$$a \sim \frac{I_0^2}{2\sigma h w^2}. \quad (3)$$

Thus, for a given electric current I_0 the photothermal amplitude a is proportional to the inverse of the strip width squared.

In the case of cylindrical heat flow the photothermal amplitude is proportional to the heating power per unit length of the strip: $a \sim P/l$. We obtain

$$a \sim \frac{I_0^2}{2\sigma h w}, \quad (4)$$

realizing that in contrast to one-dimensional heat flow the signal is proportional to the inverse width of the strip. These arguments do not apply to spherical heat flow from pointlike heat sources since the heating power per unit area cannot be defined in that case.

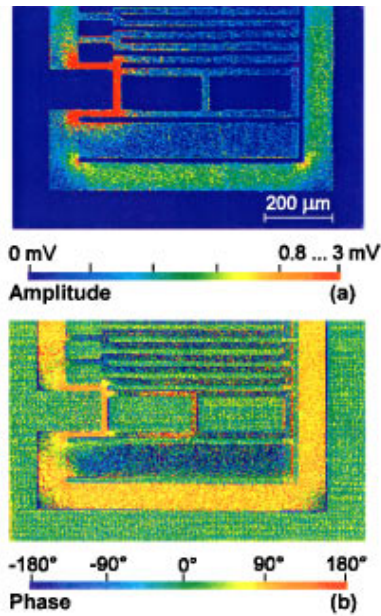


FIG. 3. (a) Amplitude and (b) phase of the photothermal response in the lower part of the microstructure. Amplitude values in the range 0.8–3 mV are all marked red to emphasize subtle effects at lower amplitude levels.

In this work we analyze heat transfer through the Al_2O_3 substrate by measuring the phase profile of a cylindrical thermal wave that can approximately be described by

$$T(r) = T_0(r) \exp\left[i\left(2\omega t - \frac{r}{L_{\text{th}}}\right)\right], \quad (5)$$

with r being the radial distance from the source and $T_0(r)$

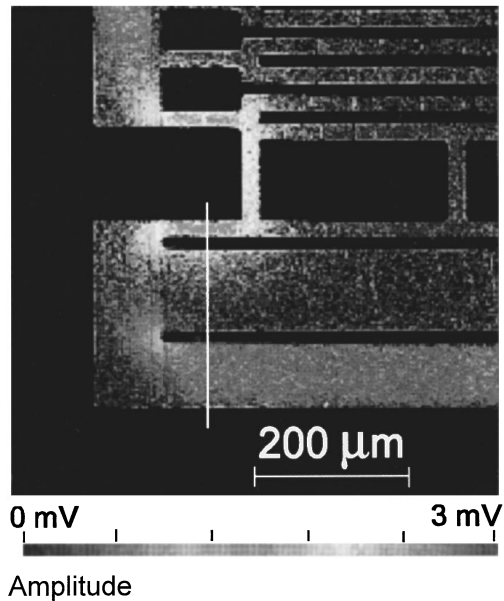


FIG. 4. Left-hand side detail of the amplitude micrograph Fig. 3(a) linearly scaled to the maximum amplitude. Here, the color scale used for the other figures was converted to a gray scale. The maximum amplitude formerly coded in red corresponds to a medium grey level while lower amplitudes formerly coded in yellow appear in white.

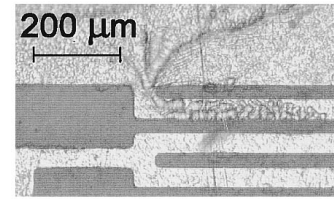


FIG. 5. Photograph of the platinum layer at the top of the test structure, partly damaged due to strong Joule heating.

the wave amplitude that is difficult to express analytically.¹⁹ The factor $\phi(r,t) = 2\omega t - r/L_{\text{th}}$ is the phase of the photothermal signal and

$$\chi = \frac{d\phi}{dr} = \frac{1}{L_{\text{th}}} = \left(\frac{2\omega}{2D}\right)^{1/2} \quad (6)$$

its slope. Plotting χ^2 as a function of the ac frequency ω we expect a straight line with slope $1/D$ and thus the procedure allows a determination of the substrate thermal diffusivity.

IV. EXPERIMENTAL RESULTS AND DISCUSSION

A. Imaging heat sources and diffusion

We scanned several areas of interest of the resistor and recorded amplitude and phase of the temperature oscillation at each point. Figures 3(a) and 3(b) present survey scans on the lower half of the resistor recorded at a modulation frequency of 1 kHz. Different values of nonvanishing current densities are distinguished by an elevated amplitude represented by the colors green, yellow, and red in Fig. 3(a); however, the phase of the photothermal signal along this path is rather constant [yellow/orange shading, Fig. 3(b)]. On sections of the platinum layer with negligible current density only a small noise amplitude with random phase was observed. From the amplitude image [Fig. 3(a)] the influence of the conducting cross section on the current density, i.e., on the amplitude of temperature oscillations, can clearly be seen. In the three narrow conducting strips appearing red an amplitude much higher than in the broad ones was measured. As the width of these strips ($20 \mu\text{m}$) is smaller than the

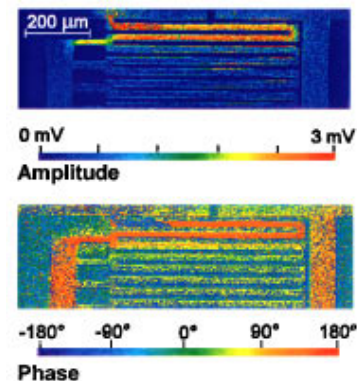


FIG. 6. (a) Amplitude and (b) phase micrograph of a part of the microstructure, where damage has occurred (see Fig. 5). The resulting decreased thermal contact of the platinum layer to the substrate results in an increased amplitude and in a strong phase contrast.

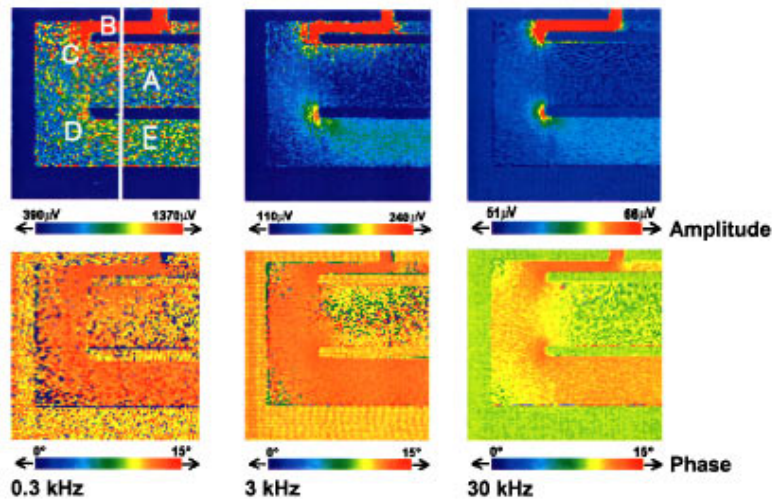


FIG. 7. Amplitude and phase micrographs recorded at 0.3, 3, and 30 kHz, demonstrating thermal wave propagation in a region with strong thermal amplitude gradients. The image represents a $300 \times 300 \mu\text{m}^2$ square in the lower left-hand side of Fig. 3.

thermal length at 1 kHz of $39 \mu\text{m}$ (see Table I) heat flow is best described by cylindrical waves. Their quantitative evaluation is described in Sec. IV B. The high-temperature oscillations on these strips causes a phase signal of high stability represented by a clear orange color in Fig. 3(b). Geometry-related effects cannot only be seen in regions of a reduced width of the platinum strip but also at the edges. There the electric current concentrates at the inner edges of right angles yielding elevated local temperature oscillations, as can be seen at the left- and right-hand-side lower corners of the structure.

Whereas in Fig. 3(a) all amplitudes between 0.8 and 3 mV are represented in red in order to visualize details in low current density areas, in Fig. 4 only the maximum amplitude values are marked with the highest level shading. Thus, Fig. 4 illustrates that in the vertical narrow conducting strip the current density is lower than in the horizontal ones, indicating that part of the current also passes through the loop that is located on the right-hand side of the three strongly heated strips. This current leads to phase values represented in orange in Fig. 3(b). An amplitude in this loop being slightly higher than in strips without flow of current can be inferred from Fig. 3(a).

The photograph in Fig. 5 displays a detail in the upper left-hand side of the resistor that was not included in the survey scan discussed previously. Due to the very high thermal load during a test experiment, part of the platinum layer in this area has melted and delaminated from the substrate. The photothermal images in Fig. 6 were recorded with the platinum resolidified at much lower current density. They give a survey of the upper half of the resistor and include the detail shown in Fig. 5. This area is particularly heated due to the high current density at the right angle of a narrow conducting strip and due to the vicinity of the lower parallel conducting strip being a heat source, as well. An elevated signal was measured on the affected platinum, due to a reduced thermal contact to the substrate. In addition, here the local phase is shifted by 180° with respect to the unaffected parts of the conducting strip. This phase contrast cannot be

explained by the reduced thermal contact, since a phase shift of about 180° between heating current and temperature oscillation is impossible. To explain this we assume that the decreased mechanical contact of the strip to the substrate allows vibrations of the platinum layer resulting in a modulated deflection of the probe beam contributing as a displacement signal and dominating its phase.

B. Detailed data analysis

We now return to the strongly heated area in the lower left-hand side corner in Fig. 3. To investigate thermal diffusion in this area we recorded amplitude and phase images at various frequencies ranging from 0.3 to 30 kHz. A series of amplitude and phase images is shown in Fig. 7 while Fig. 8 visualizes thermal wave propagation by drawing lines of equal phase for the various frequencies. The capital letters in this figure denote various areas of interest that will be discussed in the following. As no electric current passes through the broad horizontal conducting strip A forming a dead end, the temperature oscillations measured there can only be caused by thermal waves from the adjacent heated strips. These are cylindrical waves originating from the

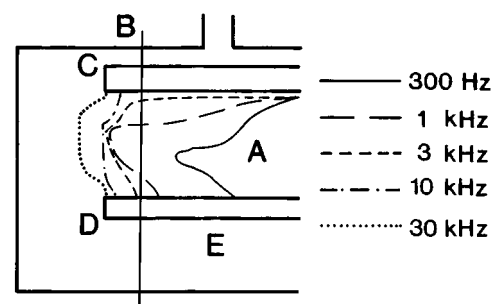


FIG. 8. Isophase lines of thermal waves in the region shown in Fig. 7 as a function of frequency. Successive lines represent a phase shift of 3° with respect to the oscillations on the conducting strip B.

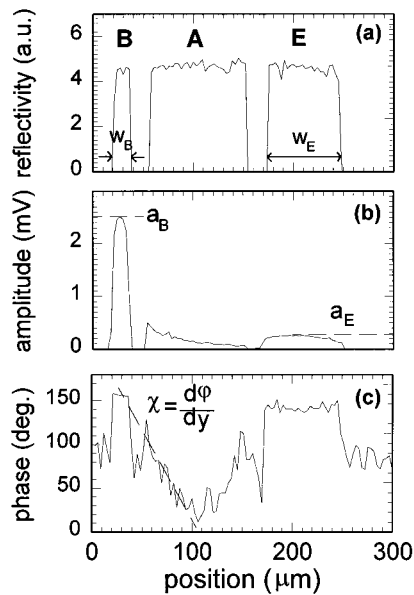


FIG. 9. Profile of probe beam reflectivity and thermoreflectance amplitude and phase at a frequency of 1 kHz measured along the vertical line shown in Figs. 4, 7, and 8. The dotted line in (c) is drawn to indicate the linear decline in phase used for diffusivity determination.

strongly heated horizontal conducting strip B and the spherical waves starting at the edges of the current path C and D. As expected, with increasing frequency these thermal waves have a shorter range in region A. At 30 kHz a nonvanishing photothermal amplitude could be measured only at the upper edge of strip A, whereas the decrease of temperature oscillations with the distance from the narrow horizontal conducting strip is obvious at 0.3 kHz. Likewise, phase images in Fig. 7 show that the phase gradient of the cylindrical wave increases with increasing frequency. The isophase lines in Fig. 8 clearly demonstrate this behavior. Similarly, the hot spot at the right angle C is best resolved at high frequencies.

For a more detailed analysis of thermal wave propagation we now investigate amplitude and phase profiles at 1 kHz measured along the white line indicated in Figs. 4, 7, and 8. The resulting cross sections shown in Fig. 9 were obtained by averaging 20 values of neighboring lines to im-

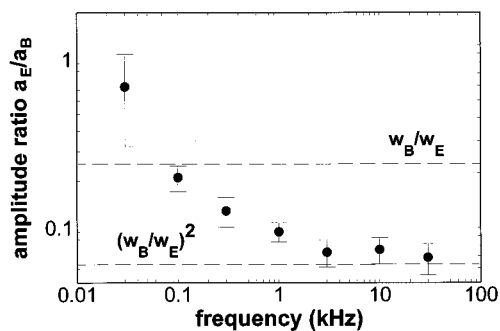


FIG. 10. Plot of the ratio of amplitudes measured on the conducting strips E and B (see nomenclature introduced in Fig. 7) as a function of frequency. The dashed lines represent the values $(w_B/w_E)^2$ and w_B/w_E expected for one- and two-dimensional diffusion, respectively.

TABLE I. Thermal lengths in the Al_2O_3 substrate.

Alternating current frequency (kHz)	Thermal length (μm)
0.03	220
0.1	123
0.3	71
1	39
3	22
10	12
30	7
100	4

prove the signal-to-noise ratio. For better clarity, we added a trace of the intensity of the reflected probe beam [Fig. 9(a)] clearly visualizing the narrow conducting strip B and the broad conducting strips A and E. On the conducting strips B and E approximately constant amplitudes were measured according to the homogeneous direct heating. The amplitude decreases toward the edges of the strip where, in contrast to the center of the conducting strip there is both vertical and lateral heat flow. The decay of the thermal wave excited in B is obvious in region A, while the amplitude of the wave from E is too small to be detected in this plot. In contrast, the phase plot of Fig. 9(c) shows a decrease on the left and on the right-hand half of the conducting strip A, due to thermal waves propagating from B and D, respectively. On the conducting strips B and E a constant phase was measured since these parts of the platinum layer are directly heated.

We now compare the amplitudes a_B and a_E in the center of the conducting strips B and E at frequencies in the range 0.3–30 kHz to correlate the amplitude to the dimensionality of heat flow from the strips. For this purpose in Fig. 10 we plotted a_E/a_B as a function of the frequency. Table I displays frequency-dependent thermal lengths calculated on the basis of Al_2O_3 parameters published by the manufacturer. As the thermal length for ac frequencies greater than 30 kHz is smaller than the width of the conducting strips ($w_B=20 \mu\text{m}$, $w_E=80 \mu\text{m}$) heat flow from both strips can be assumed to be fairly one-dimensional. As a consequence, due to Eq. (3) the ratio a_E/a_B is expected to be equal to the inverse ratio squared of the strip width $(w_B/w_E)^2=1/16$ in this high-frequency range. This behavior can clearly be seen in Fig. 10. With decreasing frequency the thermal length becomes larger than the width of the conducting strip B. This causes

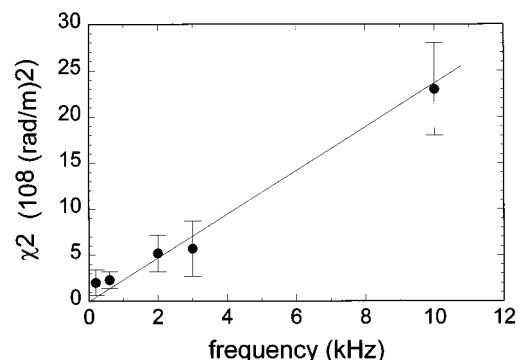


FIG. 11. Plot of the squared slope χ of the phase of the cylindrical thermal wave originating from the conducting strip B.

the thermal wave starting at B to develop a cylindrical shape, while heat flow from E is still one dimensional. Thus, B is cooled more efficiently at low frequencies explaining the increase in the ratio a_E/a_B toward low frequencies. At 0.1 kHz the thermal length ($123\ \mu\text{m}$) is greater than w_B and w_E , so that the thermal waves originating from B and E have cylindrical shapes. As a result, at this frequency Eq. (4) predicts the amplitude ratio a_E/a_B to equal w_B/w_E which is experimentally confirmed in Fig. 10. At the smallest frequency measured (0.03 kHz) the thermal length ($220\ \mu\text{m}$) is large compared to the length of the conducting strip B, which acts as a thermal point source. The resulting spherical wave cools B more efficiently, what explains the further rise of a_E/a_B toward lower frequencies. If both conducting strips were of infinite length the conducting strip B would not act as a point source compared to the thermal length. As a result $w_B/w_E=1/4$ would be the low-frequency limit of a_E/a_B .

Following the procedure described in Sec. III we have analyzed heat transfer into the Al_2O_3 substrate. For that purpose we obtained the slope χ of the phase of the cylindrical thermal wave starting at B from the fit line drawn in Fig. 9. We did so for frequencies of 0.2, 0.5, 2, 3, and 10 kHz. Although at frequencies above 3 kHz the wave originating from B is one dimensional in the near field as discussed in the preceding subsection, it has a cylindrical shape in the far field. Therefore, the high-frequency case 3 kHz does not have to be treated separately, evaluating the phase profile in the far-field region conducting strip A. We assume heat flow to take place entirely in the substrate, neglecting heat diffusion in the platinum coating and the thermal resistance between coating and substrate. This probably introduces a small systematic error. Figure 11 is the plot of χ^2 as a function of frequency. From the slope of the fit line we obtain a diffusivity of $(0.10\pm 0.03)\ \text{cm}^2/\text{s}$. This value is in agreement with the values published by the manufacturer ($D=0.074\text{--}0.098\ \text{cm}^2/\text{s}$) for the temperature range $25\text{--}500\ ^\circ\text{C}$ and confirms our hypothesis that the decrease in phase is accurately described by Eq. (6).

V. CONCLUSIONS

In this work we demonstrated a technique to image electric current densities in conducting microstructures. The method is based on thermoreflectance detection of temperature oscillations due to modulated Joule heating. We visualized the path of the electric current in strips of $20\text{--}80\ \mu\text{m}$ width clearly displaying hot spots and even thermally damaged regions that produced a signal contrast in both amplitude and phase images. Measurements at various frequencies confirmed that resolution of hot spots is best at frequencies above 10 kHz, while diffusion and thermal waves can best be

studied at lower frequencies. We imaged thermal waves of plane, cylindrical, and spherical shape and correlated the dimensionality of the waves to both conducting strip geometry and thermal length. A comparison of amplitudes on conducting strips confirmed that the ratio of thermal length to the extent of the heating surface area is crucial to the dimensionality of heat diffusion. The innovative aspect of this method to measure thermal diffusivity is the generation of a cylindrical wave with an electrically heated conducting strip. We measured the substrate diffusivity by a simple analysis of the phase profile on a micrometer scale and thereby confirmed the validity of the simple equation describing cylindrical wave propagation.

ACKNOWLEDGMENTS

This work was supported by the BriteEuram II project DAITM of the commission of the European Community. We gratefully acknowledge continued encouragement and support by E. Matthias and sample preparation and support by Jumo, M. K. Kuchheim GmbH & Co, Fulda.

- ¹H. K. Wickramasinghe, Y. Martin, D. A. H. Spear, and E. A. Ash, *J. Phys. (Paris) Colloq.* **10**, C6-191 (1983).
- ²J. T. Fanton and G. S. Kino, *Appl. Phys. Lett.* **51**, 66 (1987).
- ³E. Welsch, M. Reichling, C. Göbel, D. Schäfer, and E. Matthias, *Appl. Phys. Lett.* **61**, 916 (1992).
- ⁴U. Seidel, K. Haupt, H. G. Walther, J. Burt, and B. K. Bein, *J. Appl. Phys.* **75**, 4396 (1994).
- ⁵U. Seidel, K. Haupt, H. G. Walther, J. Burt, and M. Munidasa, *J. Appl. Phys.* **78**, 2050 (1995).
- ⁶Jian-wen Fang, Yao-chun Shen, Yue-sheng Lu, Jian-chun Cheng, and Shu-yi Zhang, in *Acoustical Imaging*, edited by Y. Wei and B. Gu (Plenum, New York, 1993), Vol. 20, p. 321.
- ⁷A. Mandelis, A. Williams, and E. K. M. Siu, *J. Appl. Phys.* **63**, 92 (1988).
- ⁸B. C. Forget and D. Fournier, *Mater. Sci. Eng. B* **24**, 199 (1994).
- ⁹B. C. Forget and D. Fournier, in *Photoacoustic and Photothermal Phenomena III*, edited by D. Bicanic, Springer Series in Optical Science, Vol. 69 (Springer, Berlin, 1992), p. 375.
- ¹⁰A. M. Mansanares, D. Fournier, and A. C. Boccara, *Electron. Lett.* **29**, 2045 (1993).
- ¹¹M. Bertolotti, G. L. Liakhov, R. Li Voti, C. Sibilgia, A. Sybru, and R. P. Wang, *Appl. Phys. Lett.* **65**, 2266 (1994).
- ¹²W. Claeys, F. Giroux, S. Dilhaire, C. Gounelle, V. Quintard, and P. Morini, *Proc. SPIE* **2090**, 197 (1993).
- ¹³W. Claeys, S. Dilhaire, and V. Quintard, *Microelectron. Eng.* **24**, 411 (1994).
- ¹⁴T. Damm, R. Gutewort, U. Stamm, and K. Friedrich, *Int. J. Optoelectron.* **7**, 181 (1992).
- ¹⁵H. K. Heinrich, B. R. Hemenway, K. A. McGroddy, and D. M. Bloom, *Electron. Lett.* **22**, 650 (1986).
- ¹⁶J. Opsal, A. Rosencwaig, and D. L. Willenborg, *Appl. Opt.* **22**, 3169 (1983).
- ¹⁷A. Rosencwaig, J. Opsal, W. L. Smith, and D. L. Willenborg, *Appl. Phys. Lett.* **46**, 1013 (1985).
- ¹⁸H. S. Carslaw and J. C. Jaeger, *Conduction of Heat in Solids* (Oxford University Press, London, 1959), Chap. 1.
- ¹⁹Reference 18, Chap. 7.